Bounding energy growth in frictionless stochastic oscillators

Michał Mandrysz[*] and Bartłomiej Dybiec[†]
Institute of Theoretical Physics, and Mark Kac Center for Complex Systems Research, Jagiellonian University, ul. St. Łojasiewicza 11, 30–348 Kraków, Poland

(Received 14 February 2020; accepted 16 July 2020; published 7 August 2020)

This paper presents analytical and numerical results on the energetics of nonharmonic, undamped, single-well, stochastic oscillators driven by additive Gaussian white noises. The absence of damping and the action of noise are responsible for the lack of stationary states in such systems. We explore the properties of average kinetic, potential, and total energies along with the generalized equipartition relations. It is demonstrated that in frictionless dynamics, nonequilibrium stationary states can be produced by stochastic resetting. For an appropriate resetting protocol, the average energies become bounded. If the resetting protocol is not characterized by a finite variance of renewal intervals, stochastic resetting can only slow down the growth of the average energies but it does not bound them. Under special conditions regarding the frequency of resets, the ratios of the average energies follow the generalized equipartition relations.

DOI: 10.1103/PhysRevE.102.022105

I. INTRODUCTION

The energetic properties of stochastic dynamical systems [1] are determined by the interplay between random forces (fluctuations) and damping (dissipation) [2,3]. For damped motions in single-well potentials perturbed by Gaussian white noise, stationary states always exist [4,5]. They are given by the Boltzmann-Gibbs (BG) distribution, which is characterized by finite average energies determined by the system temperature. BG distribution is an example of elliptical distribution because its isolines correspond to constant energy curves, which for the harmonic potential are given by ellipses. In systems with BG stationary state, ratios of average energies follow generalized equipartition relations [6–8]. Here, we study frictionless dynamics in general single-well potentials under the action of the Gaussian white noise using stochastic [4,9,10] and analytical methods [11]. Due to the absence of damping, pumping of the energy by noise is not counterbalanced by dissipation. Therefore, average energies continuously grow in an unbounded manner. Such unbounded growth of average energies is also responsible for the absence of stationary states in frictionless stochastic oscillators.

The most popular way to counterbalance the pumping of energy is by damping. In the absence of damping, there is usually no mechanism that can dissipate the harvested energy. Nevertheless, models of frictionless dynamics [12–14,14] or those that result in frictionless dynamics [15] are also studied. It is worthwhile to underline that the presence of damping might be insufficient to bound the system energy. For example, in systems driven by Lévy noises [16,17], despite the existence of the nonequilibrium stationary state [18,19], the average energy can diverge [20,21].

To exclude unlimited energy growth in frictionless dynamics, we suggest a mechanism of bounding the system energy that is based on stochastic resetting [22,23]. Stochastic resetting, mainly of position, is especially important in diffusion processes [23–25], search processes [26–28], and multiplicative processes [29]. In the context of current research, important applications of stochastic resetting include first-passage time problems [23,30] and diffusion in potential landscapes [31]. According to the Sparre-Andersen theorem [32–34] for a free stochastic process driven by symmetric, Markovian noise, the first-passage time density from the real half line follows universal $t^{-3/2}$ asymptotics. The heavy-tailed asymptotics of first-passage time density explains why the mean first-passage time of a free particle to a given target (point) diverges. Stochastic resetting can, by excluding infinite excursions, make the mean first-passage time finite [23,30]. Typically, in inverse single-well potentials there is no stationary state, because there is no mechanism that can suppress the escape of particles to infinity. Here again, stochastic resetting, which moves a particle back to a fixed point x_r, can produce nonequilibrium stationary states in unstable potentials [31]. Produced stationary states are of nonequilibrium type because resetting moves particles from all points other than x_r and introduces a source of probability at the fixed point x_r.

Following the lines of investigations utilized in [23,30,31], we use the mechanism of stochastic resetting to bound unlimited energy growth during frictionless dynamics in single-well potentials. It is assumed that resets are performed at random time instants, while the times between two consecutive resets are independent, identically distributed random variables following a one-sided probability density. During each reset, we set the system energy to zero by resetting its velocity and position. We show that for an appropriate resetting protocol, i.e., for fine-tuned renewal time distributions, the average energies can saturate at any preselected level. Moreover, despite the fact that nonequilibrium stationary states are not of BG type, we study the conditions under which average energies satisfy

[*]michal.mandrysz@student.uj.edu.pl
[†]bartek@th.if.uj.edu.pl

generalized equipartition relations [8]. If renewal intervals are characterized by diverging variance, stochastic resetting is not sufficient to reintroduce stationary states. In such a case, we observe a generic slow down of the growth rate of the average energies. Here again we demonstrate that the generalized equipartition relations can be recovered also in situations when stationary states do not exist.

Within the current paper, we study undamped (frictionless) motion in a single-well potential of x^{2n} ($n > 0$) type under the action of one or two Gaussian white noise sources. We build upon the research initiated in [35] and continued in [36], with special attention given to generalized equipartition relations [8] and the mechanism of bounding energy growth based on stochastic resetting [23,31]. The model under study, the basic theory, and the main results are presented in Sec. II. The paper is closed in Sec. III with a summary, and supplemented in Appendix.

II. MODEL AND RESULTS

Noise perturbed motion in a symmetric single-well potential

$$V(x) = k\frac{x^{2n}}{2n} \quad (k > 0, n > 0) \tag{1}$$

is described by the Langevin [5] equation

$$m\frac{d^2x(t)}{dt^2} = -\gamma m\frac{dx(t)}{dt} - kx^{2n-1}(t) + \sqrt{2\gamma k_B T m}\xi(t), \tag{2}$$

where $x(t)$ represents the position, m is the particle mass, T is the system temperature, k_B is the Boltzmann constant, and γ is a damping coefficient. In Eq. (2), $\xi(t)$ stands for the Gaussian white noise (GWN) satisfying

$$\langle \xi(t)\rangle = 0 \quad \text{and} \quad \langle \xi(t)\xi(s)\rangle = \delta(t-s). \tag{3}$$

The special case of $n = 1$ corresponds to the harmonic oscillator [37,38], while $n > 1$ corresponds to anharmonic setups. In most general situations, n does not need to be an integer; in such a case, it is necessary to replace x with $|x|$.

The system evolution is perturbed by the Gaussian white noise, which describes interactions of the oscillator with the thermal bath characterized by the temperature T. The action of noise makes the position and velocity random variables. The probability density $P(x, v; t)$, which is the probability of finding the system in a state characterized by $(x(t), v(t))$, evolves according to the diffusion (Kramers) equation [39,40]

$$\partial_t P(x,v;t) = \left[\partial_v\left(\gamma v + \frac{V'(x)}{m}\right) - v\partial_x + \gamma\frac{k_B T}{m}\partial_v^2\right]P(x,v;t). \tag{4}$$

Equation (4) has the stationary solution that exists for any potential $V(x)$, such that $V(x) \to \infty$ as $x \to \pm\infty$. It is of the Boltzmann-Gibbs (BG) type,

$$P(x,v) \propto \exp\left[-\frac{1}{k_B T}\left(\frac{mv^2}{2} + V(x)\right)\right]. \tag{5}$$

The exponent in Eq. (5) is the total energy $\mathcal{E}$, which is the sum of kinetic $\mathcal{E}_k$ and potential $\mathcal{E}_p$ energies. The total system energy $\mathcal{E} = \mathcal{E}_k + \mathcal{E}_p = \frac{1}{2}mv^2 + k\frac{x^{2n}}{2n}$ depends on its state $(x(t), v(t))$. Consequently, instantaneous energies, analogous to state variables, are random variables. Nevertheless for large t, stationary density is reached and average energies attain constant values. In the stationary state, the position and the velocity are statistically independent as Eq. (5) factorizes into the product of space-dependent and velocity-dependent parts. Moreover, Eq. (2) assures that the stochastic harmonic oscillator, corresponding to $n = 1$, fulfills the equipartition theorem [39,40]. Finally, from Eq. (5), for any n, one can calculate

$$\langle \mathcal{E}_k\rangle = \iint \frac{1}{2}mv^2 P(x,v)dx\,dv = \frac{1}{2}k_B T, \tag{6}$$

$$\langle \mathcal{E}_p\rangle = \iint k\frac{x^{2n}}{2n}P(x,v)dx\,dv = \frac{1}{2n}k_B T, \tag{7}$$

and

$$\langle \mathcal{E}\rangle = \iint \left[\frac{1}{2}mv^2 + k\frac{x^{2n}}{2n}\right]P(x,v)dx\,dv = \frac{n+1}{2n}k_B T. \tag{8}$$

From Eqs. (6), (7) and (8), one obtains

$$\frac{\langle \mathcal{E}_k\rangle}{\langle \mathcal{E}\rangle} = \frac{n}{1+n} \tag{9}$$

and

$$\frac{\langle \mathcal{E}_p\rangle}{\langle \mathcal{E}\rangle} = \frac{1}{1+n}. \tag{10}$$

The very same formulas [see Eqs. (6) and (7)] have also been derived in [41], where undamped, classical, fully deterministic, anharmonic oscillators with $V(x)$ given by Eq. (1) have been studied. In other words, for undamped, classical, conservative oscillators, time-averaged kinetic and potential energies are also given by Eqs. (6) and (7). An alternative derivation, for the general nonlinear oscillator with the parametric noise, is presented in Ref. [8]. Moreover, in accordance with the virial theorem [42],

$$\frac{\langle \mathcal{E}_k\rangle}{\langle \mathcal{E}_p\rangle} = n. \tag{11}$$

In this work, we are interested in modifications of the general model described by Eq. (2). More precisely, we are still studying the system described by Eq. (2) with the $V(x)$ given by Eq. (1) assuming frictionless dynamics, i.e., dynamics corresponding to $\gamma = 0$. Nevertheless, for clarity of presentation, we start with a discussion of the full, damped dynamics. For the purpose of deriving the quantities of interest, Eq. (2) can be rewritten as a set of two first-order equations:

$$\begin{aligned}\frac{dx(t)}{dt} &= v(t),\\ \frac{dv(t)}{dt} &= -\gamma v(t) - \omega^2 x^{2n-1}(t) + \sqrt{h_v}\xi(t),\end{aligned} \tag{12}$$

where $\omega^2 = k/m$ and $h_v = 2\gamma k_B T/m$. In Eqs. (12) the noise term is present in the second equation only. Additionally, we assume that also the first equation is subjected to the action of noise [43]. Such an extension allows for larger generality than typically studied situations described by Eqs. (12). In particular, two noise sources allow for a study of symmetries of solutions of Eqs. (13) especially for the harmonic potential.

Finally, Eqs. (12) take the following form:

$$\frac{dx(t)}{dt} = v(t) + \sqrt{h_x}\xi_x(t),$$
$$\frac{dv(t)}{dt} = -\gamma v(t) - \omega^2 x^{2n-1}(t) + \sqrt{h_v}\xi_v(t). \quad (13)$$

The evolution of the probability density $P(x, v; t)$ for the system described by Eqs. (13) is provided by the diffusion equation, which differs from Eq. (4) by the presence of the additional ∂_x^2 term; see Ref. [40]. Consequently, stationary states for the model described by Eqs. (13) cannot be of BG type.

From Eqs. (13) it is possible to derive equations describing the time evolution of the average kinetic $\langle \mathcal{E}_k \rangle$ and potential $\langle \mathcal{E}_p \rangle$ energies; see Appendix. The time derivatives of the average energies are given by

$$\frac{d}{dt}\langle \mathcal{E}_p \rangle = k\langle x^{2n-1} v \rangle + \frac{1}{2} h_x k(2n-1)\langle x^{2n-2} \rangle \quad (14)$$

and

$$\frac{d}{dt}\langle \mathcal{E}_k \rangle = -m\gamma \langle v^2 \rangle - m\omega^2 \langle x^{2n-1} v \rangle + \frac{1}{2} m h_v, \quad (15)$$

while the evolution of the total energy is described by

$$\frac{d}{dt}\langle \mathcal{E} \rangle = \frac{d}{dt}\langle \mathcal{E}_p + \mathcal{E}_k \rangle = -m\gamma \langle v^2 \rangle + \frac{1}{2} h_x k(2n-1)\langle x^{2n-2} \rangle + \frac{1}{2} m h_v. \quad (16)$$

A. Unbounded energy growth in the frictionless case

For $\gamma > 0$, energy growth saturates at a stationary value, which is proportional to the system temperature. In the frictionless case, i.e., for $\gamma = 0$, a different situation takes place and average energies grow in an unbounded manner [36]. For $n = 1$, the system described by Eq. (2) or Eqs. (13) can be studied analytically [12,40,44,45]. For the parabolic potential, these equations are linear, and thus standard methods of solving linear differential equations can be applied [40,44]. For $x(0) = 0$, $v(0) = 0$, the following formulas can be derived:

$$\langle \mathcal{E}_k(t) \rangle = \frac{1}{2} m \langle v^2 \rangle = h_x \frac{2kt - m\omega \sin(2\omega t)}{8} + h_v \frac{2m\omega t + m \sin(2\omega t)}{8\omega} = \frac{1}{4}[h_x k + h_v m]t + \frac{1}{8}\sin(2\omega t)\left[\frac{h_v m}{\omega} - h_x m\omega\right] \quad (17)$$

and

$$\langle \mathcal{E}_p(t) \rangle = \frac{1}{2} m\omega^2 \langle x^2 \rangle = \frac{1}{2} k \langle x^2 \rangle = h_x \frac{2kt + m\omega \sin(2\omega t)}{8} + h_v \frac{2m\omega t - m \sin(2\omega t)}{8\omega} = \frac{1}{4}[h_x k + h_v m]t + \frac{1}{8}\sin(2\omega t)\left[h_x m\omega - \frac{h_v m}{\omega}\right], \quad (18)$$

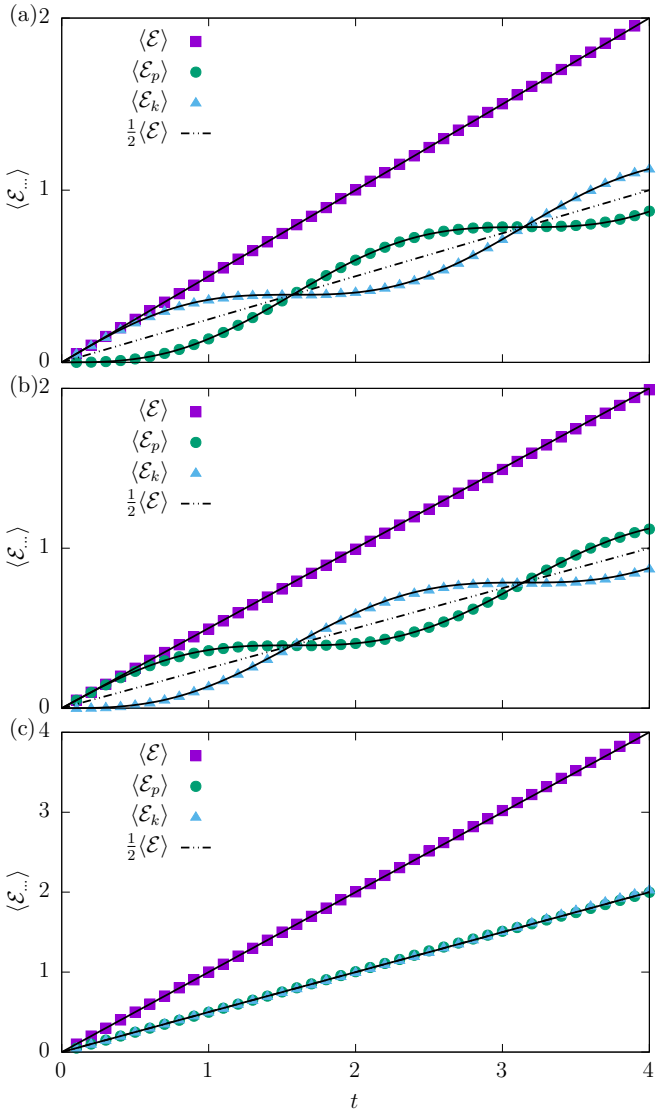

FIG. 1. Time dependence of average energies for the frictionless, uninterrupted motion in the parabolic potential ($n = 1$) with $(h_x, h_v) = (0, 1)$ [top panel, (a)], $(h_x, h_v) = (1, 0)$ [middle panel, (b)], and $(h_x, h_v) = (1, 1)$ [bottom panel, (c)]. Other parameters: $k = 1$ and $m = 1$. Solid lines present theoretical formulas [see Eqs. (17)–(19)] while the dot-dashed line presents $\langle \mathcal{E}(t) \rangle/2$ [see Eqs. (21) and (22)].

giving rise to

$$\langle \mathcal{E}(t) \rangle = \langle \mathcal{E}_k(t) \rangle + \langle \mathcal{E}_p(t) \rangle = \left[\frac{h_x k}{2} + \frac{h_v m}{2}\right] t, \quad (19)$$

where $\omega = \sqrt{k/m}$. The presence of the additional noise ξ_x in the first line of Eqs. (13) increases the slope of the linear growth of average energy. Alternatively, Eqs. (17) and (18) can also be derived using equations for moments; see Eq. (23). Finally, Eq. (19) can be easily derived from Eq. (16), because for the harmonic oscillator $\langle x^{2n-2} \rangle = \langle 1 \rangle = 1$. Such an approach was used in [36], where the $h_x = 0$ case was studied.

For the parabolic potential ($n = 1$) in the frictionless, uninterrupted motion, the linear growth of the average energies is clearly visible in Fig. 1, which depicts results for $\omega = 1$

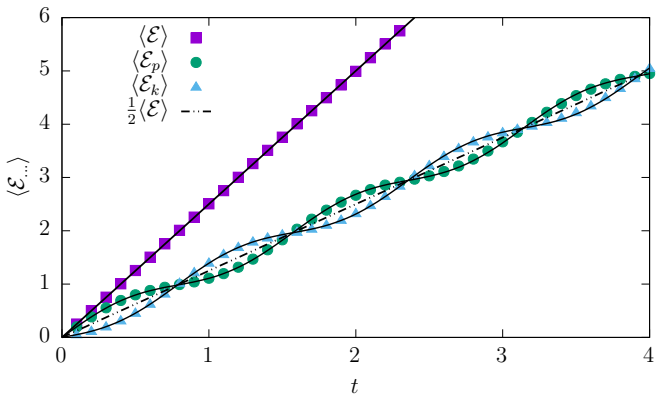

FIG. 2. The same as in Fig. 1(c) for $k = 4$ and $m = 1$. Solid lines present theoretical formulas; see Eqs. (17)–(19). The dot-dashed line presents $\langle\mathcal{E}(t)\rangle/2$; see Eqs. (21) and (22).

and various values of h_x and h_v. The purely linear growth of the average kinetic and potential energies (see the bottom panel of Fig. 1) is recorded due to a very special choice of ω. The special choice of k and m assures that the change in (h_x, h_v) from (0,1) to (1,0) results in a simple exchange of the average kinetic energy with the average potential energy. This symmetry results in the absence of oscillations (equal average energies) at all times, i.e., $\langle\mathcal{E}_k(t)\rangle = \langle\mathcal{E}_p(t)\rangle$ for $(h_x, h_v) = (1, 1)$. In more general situations, this does not occur and hence $\langle\mathcal{E}_k(t)\rangle$ and $\langle\mathcal{E}_p(t)\rangle$ follow oscillatory growth along the linear trend; see Eqs. (17) and (18) and Fig. 2. Nevertheless, playing with the system's parameters, it is possible to control which type of energy dominates at short times. For example, for $h_x = 0$, initially $\langle\mathcal{E}_k(t)\rangle$ is always larger than $\langle\mathcal{E}_p(t)\rangle$, while for $h_v = 0$ the average potential energy dominates; compare the top and middle panels of Fig. 1. Moreover, for $n = 1$, the average total energy grows linearly regardless of ω; see Eq. (19) and Figs. 1 and 2.

Contrary to the harmonic potential, for nonharmonic potentials the average total energy grows linearly for $h_x = 0$ only. This follows directly from Eq. (16), which gives

$$\langle\mathcal{E}(t)\rangle = \frac{h_v m}{2} \times t + \mathcal{E}_0. \tag{20}$$

Moreover, in [46] the weak convergence of the scaled energy process $\mathcal{E}(t)/t$ was proven, and the scaled stationary probability density $P_{st}(x/t^{1/2n}, v/t^{1/2})$ was derived; see also [13,36].

As an exemplary nonharmonic setup, we show results for the quartic ($n = 2$) potential. In the top panel of Fig. 3, the predicted linear growth of $\langle\mathcal{E}(t)\rangle$ is observed as $h_x = 0$. In the remaining panels, the average energies grow superlinearly due to the presence of the $\langle x^{2n-2}\rangle = \langle x^2\rangle$ term; see Eq. (16). From fits, we see that the growth is quadratic. In all the above cases, after the disappearance of the transient (usually oscillatory) behavior, generalized equipartition relations hold [see Eqs. (9) and (10) and Refs. [8,41]], i.e.,

$$\langle\mathcal{E}_k\rangle = \frac{n}{1+n}\langle\mathcal{E}\rangle \tag{21}$$

and

$$\langle\mathcal{E}_p\rangle = \frac{1}{1+n}\langle\mathcal{E}\rangle. \tag{22}$$

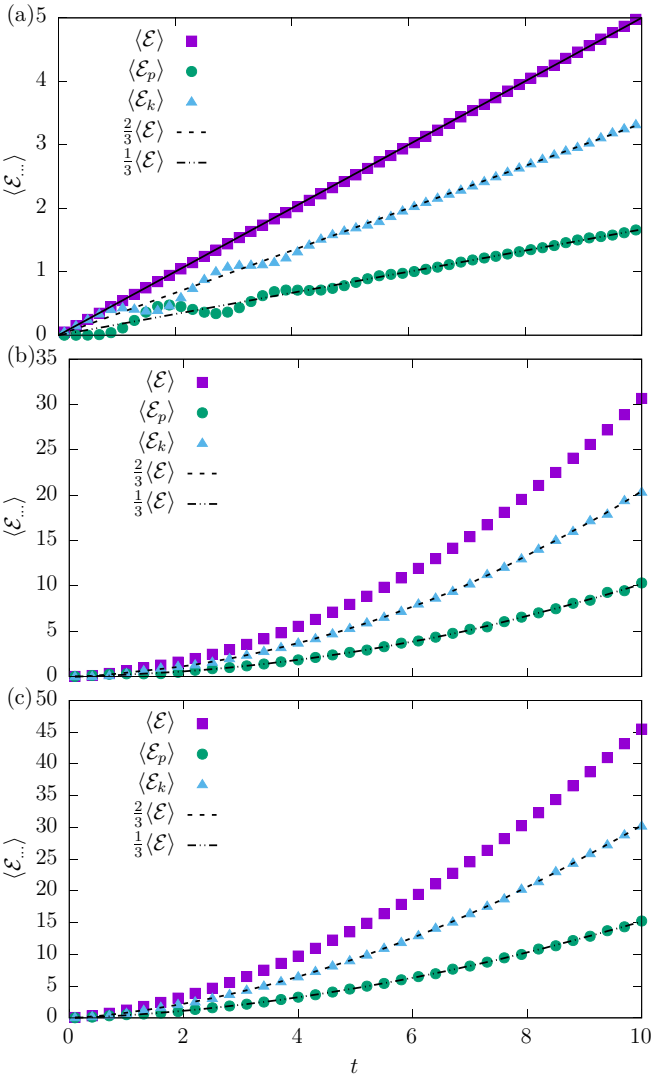

FIG. 3. Time dependence of average energies for the frictionless, uninterrupted motion in the quartic potential ($n = 2$) with $(h_x, h_v) = (0, 1)$ [top panel, (a)], $(h_x, h_v) = (1, 0)$ [middle panel, (b)], and $(h_x, h_v) = (1, 1)$ [bottom panel, (c)]. Other parameters: $k = 1$ and $m = 1$. The solid line in the top panel depicts the theoretical linear scaling of the average total energy $\langle\mathcal{E}(t)\rangle$; see Eq. (19). Dashed and dot-dashed lines present $\frac{2}{3}\langle\mathcal{E}(t)\rangle$ and $\frac{1}{3}\langle\mathcal{E}(t)\rangle$ scalings; see Eqs. (21) and (22).

In Fig. 3, scalings predicted by Eqs. (21) and (22) with $n = 2$ are depicted with dashed and dot-dashed lines. These scalings hold not only for the typical noise-driven dynamics, i.e., $(h_x, h_v) = (0, 1)$, but also for $(h_x, h_v) = (1, 1)$ and $(h_x, h_v) = (1, 0)$.

For the parabolic ($n = 1$) potential, from Eqs. (17)–(19) one can calculate the asymptotic ($t \to \infty$) ratio of the average energies: $\langle\mathcal{E}_k(\infty)\rangle/\langle\mathcal{E}(\infty)\rangle = \langle\mathcal{E}_p(\infty)\rangle/\langle\mathcal{E}(\infty)\rangle = 1/2$, which, for large but finite t, agrees with predictions of Eqs. (21) and (22). Deviations from Eqs. (21) and (22) are visible for small t because of the periodic addition to the linear trend; see Eqs. (17)–(19) and Figs. 1 and 2. The very same situation takes place for the quartic ($n = 2$) potential; see Fig. 3. Dashed and dot-dashed lines in Fig. 3 present

numerically calculated $\langle \mathcal{E}(t) \rangle$ multiplied by factors obtained from Eqs. (21) and (22), i.e., $\langle \mathcal{E}(t) \rangle \times n/(1+n)$ and $\langle \mathcal{E}(t) \rangle \times 1/(1+n)$ with $n = 2$. Expected values of the average kinetic and potential energies agree very well with these predictions.

B. Bounding unlimited energy growth

For $\gamma > 0$, the total energy for the model described by Eqs. (13) is limited. For $h_x = 0$, the model is equivalent to the standard underdamped Langevin equation (2), and the stationary density is given by the BG distribution (5). For $h_x > 0$, the stationary density still exists, which is clearly visible from computer simulations (results not shown). Alternatively, one can use the equation for moments $\langle x^{2n} \rangle$, $\langle v^2 \rangle$, ... For instance, for $n = 1$ one has

$$\begin{aligned} \frac{d}{dt}\langle x^2 \rangle &= 2\langle xv \rangle + h_x, \\ \frac{d}{dt}\langle v^2 \rangle &= -2\gamma \langle v^2 \rangle - 2\omega^2 \langle xv \rangle + h_v, \\ \frac{d}{dt}\langle xv \rangle &= \langle v^2 \rangle - \gamma \langle xv \rangle - \omega^2 \langle x^2 \rangle \end{aligned} \tag{23}$$

from which Eqs. (17) and (18) can also be derived. Moreover, from Eq. (23) stationary values of moments $\langle x^2 \rangle$, $\langle v^2 \rangle$, and $\langle xv \rangle$ can be calculated as

$$\begin{aligned} \langle x^2 \rangle_\infty &= \frac{h_x(\gamma^2+\omega^2)+h_v}{2\gamma\omega^2}, \\ \langle v^2 \rangle_\infty &= \frac{h_x\omega^2+h_v}{2\gamma}, \\ \langle xv \rangle_\infty &= -\frac{h_x}{2}. \end{aligned} \tag{24}$$

The set of equations for $V(x) \propto x^{2n}$ with $n > 1$ is more complicated than for $n = 1$. The increasing complexity is because of higher-order terms, e.g., $\langle x^{2n} \rangle$ and $\langle x^{2n-1}v \rangle$; see Eqs. (14) and (15). For instance, the formula for the time derivative of $\langle x^{2n-1}v \rangle$ takes the following form:

$$\begin{aligned} \frac{d}{dt}\langle x^{2n-1}v \rangle &= (2n-1)\langle x^{2n-2}v^2 \rangle \\ &\quad + \frac{1}{2}h_x(2n-1)(2n-2)\langle x^{2n-3}v \rangle \\ &\quad - \gamma \langle x^{2n-1}v \rangle - \omega^2 \langle x^{4n-2} \rangle, \end{aligned} \tag{25}$$

because $d(x^{2n-1}v) = (2n-1)x^{2n-2}v\,dx + \frac{1}{2}(2n-1)(2n-2)x^{2n-3}v(dx)^2 + x^{2n-1}dv$ and Eqs. (A3) and (A5). Consequently, subsequent equations have to be introduced, making the system of equations infinite. This should be contrasted with the numerically estimated total average energy $\langle \mathcal{E}(t) \rangle$ and moments $\langle v^2 \rangle \propto \langle \mathcal{E}_k \rangle$, $\langle x^{2n} \rangle \propto \langle \mathcal{E}_p \rangle$, which for the frictionless dynamics in the quartic potential, i.e., $n = 2$, grow linearly or quadratically in time; see Fig. 3.

In the damped case, i.e., $\gamma > 0$, the linear restoring force corresponding to $n = 1$ [see Eqs. (23) and (24)] is sufficient to assure the existence of a stationary state. More precisely, velocity is bounded due to damping, while position is constrained by the restoring force. For steeper potentials than parabolic, i.e., $n > 1$, the restoring force is stronger, making the system localized in a smaller fraction of space. In the limit of $n \to \infty$, the potential well [see Eq. (1)] transforms into an infinite rectangular potential well producing the marginal $P(x)$ density uniform.

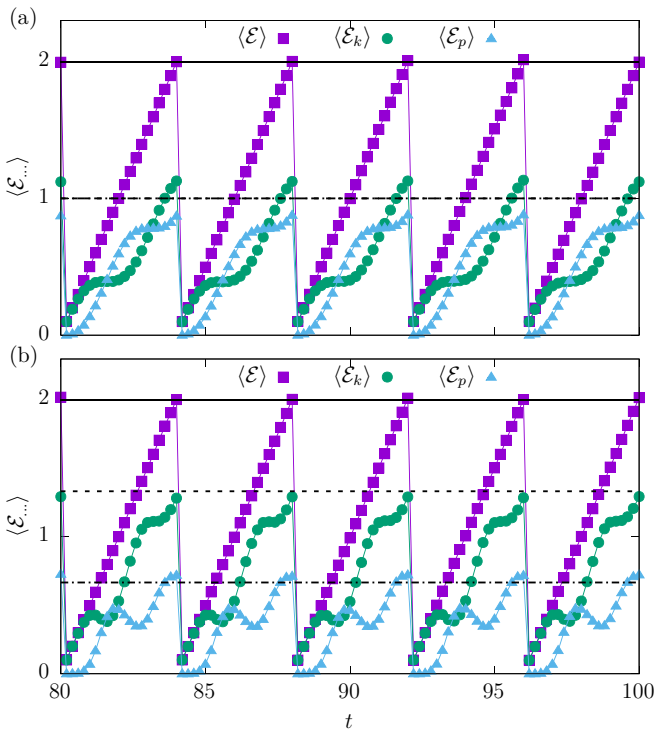

FIG. 4. Time dependence of average energies for the parabolic [top panel, (a)] and quartic [bottom panel, (b)] potentials with $(h_x, h_v) = (0, 1)$. The reset is performed every $\tau = 4$, i.e., $f(\tau) = \delta(\tau - 4)$. Other parameters: $k = 1$ and $m = 1$. Solid, dashed, and dot-dashed lines present $\langle \mathcal{E} \rangle_{\max}$ with $\frac{1}{2}\langle \mathcal{E} \rangle_{\max}$, $\frac{1}{2}\langle \mathcal{E} \rangle_{\max}$ [top panel (a)], and $\langle \mathcal{E} \rangle_{\max}$ with $\frac{2}{3}\langle \mathcal{E} \rangle_{\max}$, $\frac{1}{3}\langle \mathcal{E} \rangle_{\max}$ [bottom panel (b)]; see Eqs. (21) and (22).

Contrary to the damped dynamics, in the frictionless case there is no stationary state for the model described by Eqs. (2), (12), or (13). The lack of damping allows for unbounded energy growth. Nevertheless, it is possible to introduce other mechanisms resulting in bounding of the system energy. To stop energy growth for $\gamma = 0$, we consider stochastic resetting [22,23] at random time instants. We consider the scenario in which both the velocity and the position are simultaneously reset, i.e., $v \to 0$ and $x \to 0$. We assume that the resetting is associated with the distribution $f(\tau)$ providing renewal intervals τ ($\tau > 0$) between resets [47]. Renewal intervals are independent, identically distributed random variables following a (one-sided) distribution $f(\tau)$.

In the scenario in which both velocity and position are reset, the energy is fully determined by the survival time (age) $A_t = t - t_R$, i.e., the time measured since the last reset t_R. The sequence of reset times $t_R^{(n)}$ is determined by the $f(\tau)$, i.e.,

$$t_R^{(n)} = \sum_{i=1}^{n} \tau_i, \tag{26}$$

where τ_i is the sequence of renewal intervals. As an introductory example, we start with $f(\tau) = \delta(\tau - \Delta)$, where $\delta(\cdots)$ is Dirac's delta function. Typical growth of energies $\langle \mathcal{E}(t) \rangle$, $\langle \mathcal{E}_p(t) \rangle$, and $\langle \mathcal{E}_k(t) \rangle$, interrupted by regular resets occurring every time interval Δ, can be expected. Indeed, this type of behavior is visible in Fig. 4 for the parabolic and quartic

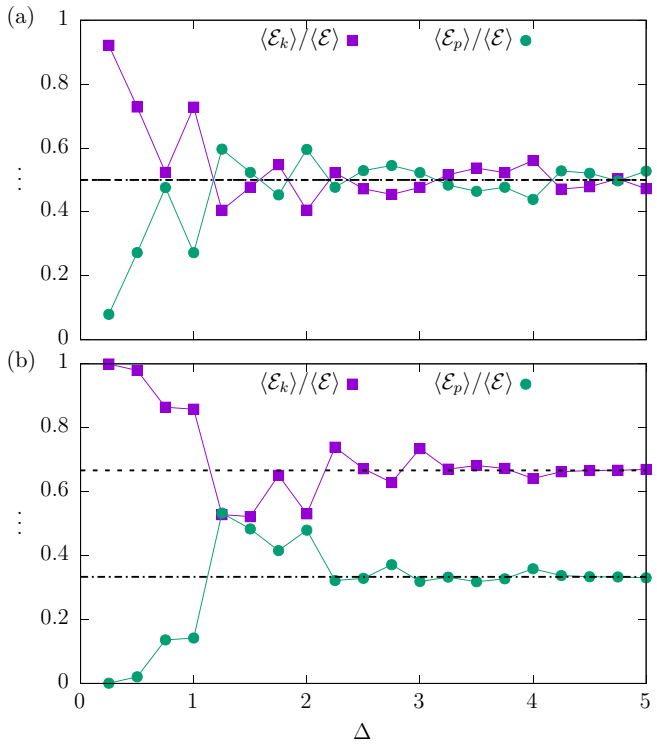

FIG. 5. Ratio of average energies $\langle\mathcal{E}_k\rangle/\langle\mathcal{E}\rangle$ and $\langle\mathcal{E}_p\rangle/\langle\mathcal{E}\rangle$ at $t=\Delta$ for the parabolic [top panel, (a)] and quartic [bottom panel, (b)] potentials with $(h_x,h_v)=(0,1)$. The reset is performed every Δ, i.e., $f(\tau)=\delta(\tau-\Delta)$. Other parameters: $k=1$ and $m=1$. Solid, dashed, and dot-dashed lines present theoretical ratios given by Eqs. (21) and (22), i.e., 1/2 [top panel, (a)] and 2/3, 1/3 [bottom panel, (b)].

potentials with $(h_x,h_v)=(0,1)$. A very similar behavior is recorded for $(h_x,h_v)=(1,0)$ and $(h_x,h_v)=(1,1)$ (results not shown). Solid lines in Fig. 4 present maximal total energies, while dashed and dot-dashed lines present maximal total energies multiplied by the prefactors from Eqs. (21) and (22), which should give maximal average kinetic and potential energies, respectively. As is visible in Fig. 4, the average kinetic and potential energies do not necessarily correspond to the given fraction of total energies. The violation of equipartition relations in the case of deterministic resets is natural—there was insufficient time for the system to lose the memory of its initial state, i.e., transient oscillations are present in between reset intervals. In Fig. 5 we present ratios of the average energies as a function of the time interval Δ between two consecutive resets. Figure 5 clearly indicates the return to generalized equipartition [scalings predicted by Eqs. (21) and (22)] in the case of large Δ. Consequently, if Δ is too small, the generalized equipartition cannot be satisfied.

The more interesting situation is recorded when resets are performed at random time instants. In such a case, in order to calculate the average energy in addition to averaging over noise realizations, it is necessary to perform additional averaging over time (age) which passed since the last reset. The rate of average energy growth is easily traceable analytically when in the absence of resetting, the average energy grows linearly in time. As we have shown in Sec. II A, such a situation takes place for $\gamma=0$ with $n=1$; see Eq. (19) or any n with $h_x=0$, i.e.,

$$\langle\mathcal{E}(t)\rangle=\Lambda t \tag{27}$$

with

$$\Lambda=\begin{cases}\frac{h_x k+h_v m}{2} & \text{for} \quad n=1,\\ \frac{h_v m}{2} & \text{for} \quad n>1, h_x=0.\end{cases} \tag{28}$$

The value of the average energy is then determined by the properties of the renewal intervals, which are the times between two consecutive resets. Here, we assume that renewal intervals τ_i are independent and identically distributed random variables following the $F(\tau)$ distribution [$f(\tau)=\frac{dF(\tau)}{d\tau}$]. After a transient period, the average energy does not depend on time if the average time since the last reset (age) is finite. The average time since the last reset $\langle A_t\rangle$ exists if the variance of renewal intervals τ is finite, i.e., $\mathrm{var}(\tau)=\langle\tau^2\rangle-\langle\tau\rangle^2<\infty$. In such a case, from the renewal theory [47], we have the following formula for $\langle A_t\rangle$:

$$\langle A_t\rangle=\frac{\langle\tau^2\rangle}{2\langle\tau\rangle}, \tag{29}$$

where $\langle\tau\rangle$ and $\langle\tau^2\rangle$ denote moments of the renewal intervals, e.g., $\langle\tau\rangle=\int_0^\infty f(\tau)\tau\,d\tau$. The average energy reads

$$\langle\mathcal{E}(t)\rangle=\Lambda\langle A_t\rangle=\Lambda\frac{\langle\tau^2\rangle}{2\langle\tau\rangle}. \tag{30}$$

Figures 6 and 7 present the time dependence of the average energies for parabolic $n=1$ (Fig. 6) and quartic $n=2$ (Fig. 7) potentials with the half-normal renewal time distribution

$$f(\tau)=\sqrt{\frac{2}{\pi\sigma_r^2}}\exp\left[-\frac{\tau^2}{2\sigma_r^2}\right]\qquad(\tau>0), \tag{31}$$

for which $\langle\tau\rangle=\sqrt{2/\pi}\sigma_r$, $\langle\tau^2\rangle=\sigma_r^2$, $\mathrm{var}(\tau)=\langle\tau^2\rangle-\langle\tau\rangle^2=(1-2/\pi)\sigma_r^2$, and most importantly $\langle A_t\rangle=\sqrt{\pi/8}\times\sigma_r$. Consequently, for $n=1$ or $h_x=0$ we have

$$\langle\mathcal{E}\rangle=\Lambda\langle A_t\rangle=\Lambda\sqrt{\frac{\pi}{8}}\sigma_r, \tag{32}$$

where Λ is given by Eq. (28). The above predictions are confirmed in Figs. 6 and 7, which present results for $n=1$ and 2, respectively. For the parabolic potential, the agreement between theoretical predictions [see Eq. (32)] and computer simulations is reached in all cases. For $(h_x,h_v)=(1,0)$ and $(h_x,h_v)=(0,1)$, the average total energies $\langle\mathcal{E}\rangle$ are the same, while for $(h_x,h_v)=(1,1)$ it is two times larger than in the former cases. For the quartic potential, we have the formula for the stationary value of $\langle\mathcal{E}\rangle$ for $h_x=0$ only (see the top panel of Fig. 7), because only for $h_x=0$ do we know the formula for $\langle\mathcal{E}(t)\rangle$ [see Eq. (28)]. For the quartic potential with $h_x>0$ (see the middle and bottom panels of Fig. 7), the average energies are also bounded. At this time, stationary values are not easily related to $\langle A_t\rangle$ because in the absence of resetting, the average energies are nonlinear functions of time; see Fig. 3. As for $n=1$, for $(h_x,h_v)=(1,1)$, due to the presence of two noise sources, the average energies attain larger values. In Figs. 6 and 7, the average energy partitions differ from the predictions of Eqs. (21) and (22).

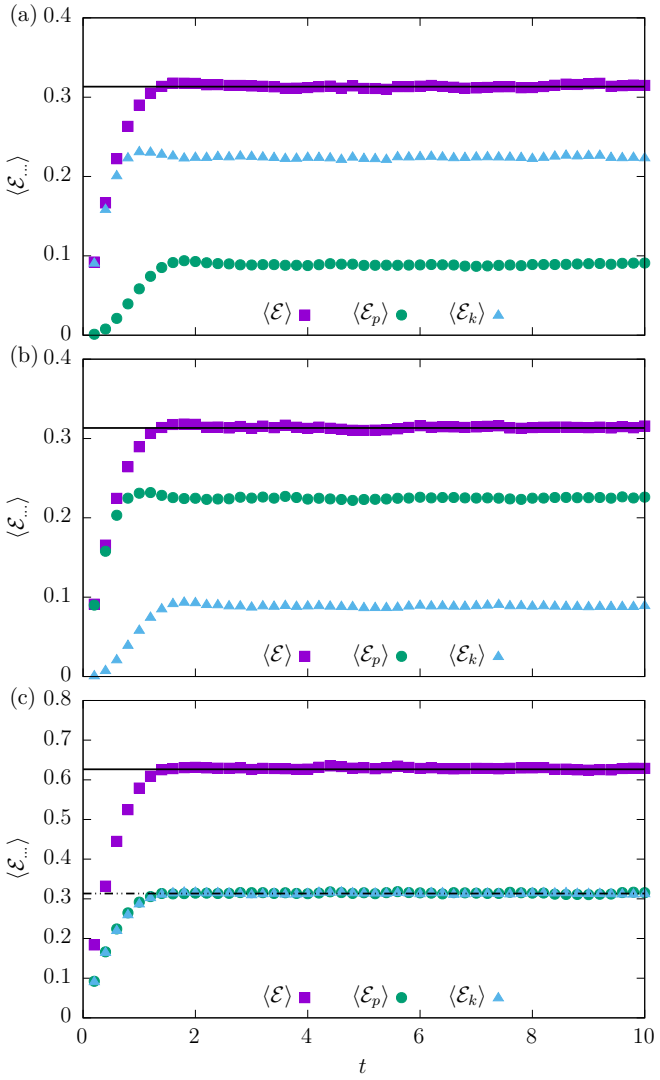

FIG. 6. Time dependence of average energies for the parabolic ($n = 1$) potential with $(h_x, h_v) = (0, 1)$ [top panel, (a)], $(h_x, h_v) = (1, 0)$ [middle panel, (b)], and $(h_x, h_v) = (1, 1)$ [bottom panel, (c)]. Renewal intervals τ are distributed according to the half-normal distribution, see Eq. (31). Different curves correspond to various types of energies $\langle \mathcal{E}(t) \rangle$, $\langle \mathcal{E}_p(t) \rangle$, $\langle \mathcal{E}_k(t) \rangle$. Solid lines depict the asymptotic energy $\langle \mathcal{E} \rangle$ given by Eq. (32), while the dash-dotted line in the bottom panel (c) shows $\frac{1}{2}\langle \mathcal{E} \rangle$. Other parameters: $m = 1$ and $k = 1$.

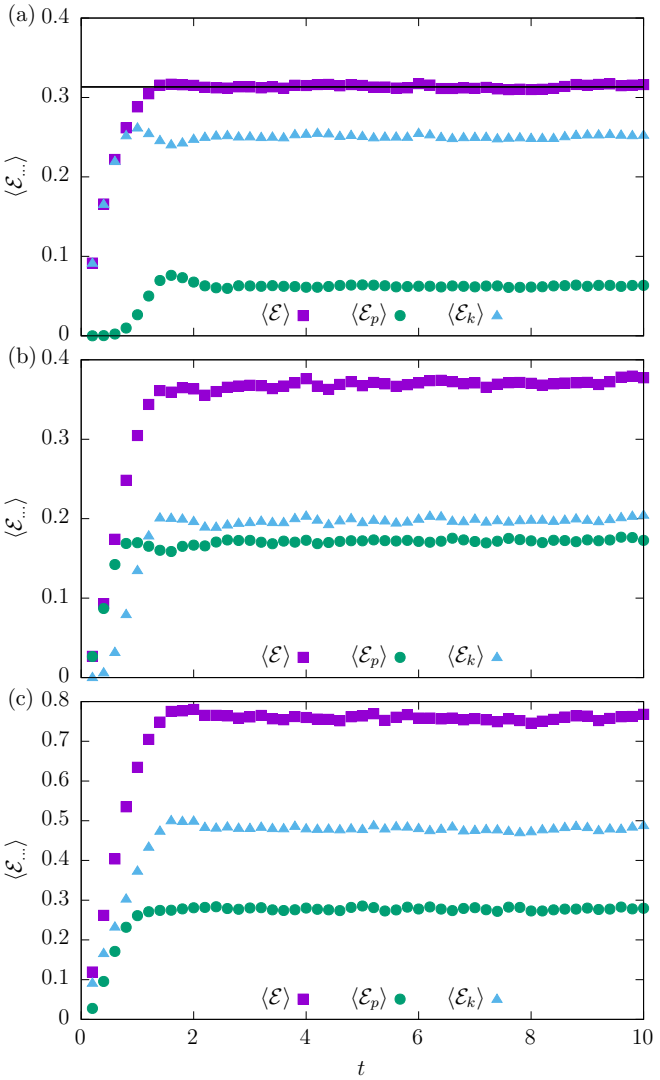

FIG. 7. The same as in Fig. 6 for the quartic ($n = 2$) potential. The solid line in the top panel (a) depicts the asymptotic energy $\langle \mathcal{E} \rangle$ given by Eq. (32).

The difference, in the case of $n = 1$, comes from regular oscillations and relatively small $\langle \tau \rangle$. In the special case of $h_x = h_v = 1$ and $m = k = 1$ when there are no oscillations (see the bottom panel of Fig. 1), the problem has not appeared; however, the equipartition was accidental (see below).

The saturation of average energies (see Figs. 6 and 7) is connected with the existence of nonequilibrium stationary states. For the parabolic potential, nonequilibrium stationary densities corresponding to Fig. 6 are depicted in Fig. 8. Various panels of Fig. 8 correspond to $(h_x, h_v) = (0, 1)$ (top left panel), $(h_x, h_v) = (1, 0)$ (top right panel), and $(h_x, h_v) = (1, 1)$ (bottom panel). If nonequilibrium stationary densities would be of BG type, these densities would be constant on the constant energy curves, i.e., they would be elliptical. In the case of $n = 1$ with $k = 1$ and $m = 1$, these ellipses should reduce to circles. Therefore, for $(h_x, h_v) = (0, 1)$ and $(h_x, h_v) = (1, 0)$, nonequilibrium stationary densities are clearly not of BG type. For $(h_x, h_v) = (1, 1)$, the nonequilibrium stationary density appears to be spherically symmetric, however this is only one of the properties of the BG distribution. To finalize our tests, we present the additional Fig. 9 with marginal densities $P(x)$ (top panel) and $P(v)$ (bottom panel). Figure 9 confirms that nonequilibrium stationary densities differ from BG type also for $(h_x, h_v) = (1, 1)$. As is clearly visible in Fig. 9, in all cases under study, decay of marginal densities $P(x)$ and $P(v)$ (points) appears to be exponential. Consequently, it differs significantly from the appropriate decay of marginal densities of the BG distribution, which for the parabolic potential is of $\exp(-bx^2)$ and $\exp(-bv^2)$ type, i.e., it is half-Gaussian. Moreover, in order to emphasize differences, additional solid lines in Fig. 9 show half-Gaussians fitted to results of simulations. Finally, we have checked that also in situations when generalized equipartition relations hold,

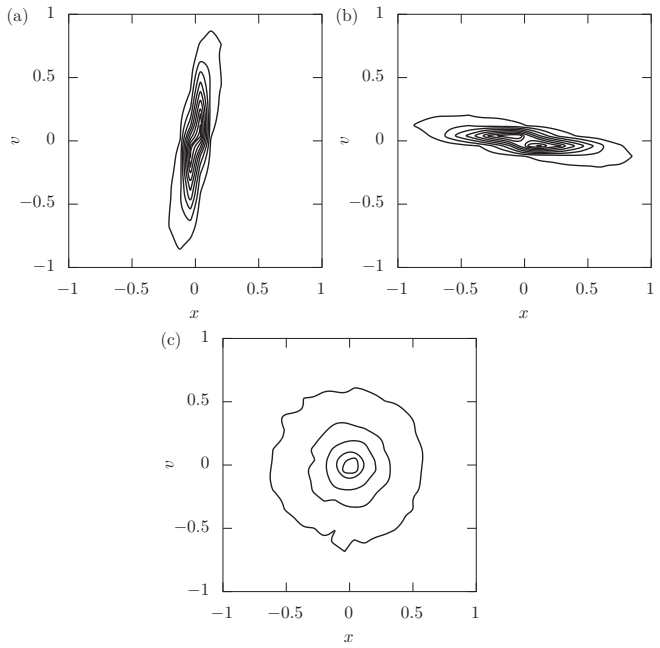

FIG. 8. Nonequilibrium stationary densities $P(x, v)$ for the parabolic ($n = 1$) potential with $(h_x, h_v) = (0, 1)$ [top left panel, (a)], $(h_x, h_v) = (1, 0)$ [top right panel, (b)], and $(h_x, h_v) = (1, 1)$ [bottom panel, (c)]. Renewal intervals τ are distributed according to the half-normal distribution, see Eq. (31). Other parameters: $m = 1$ and $k = 1$.

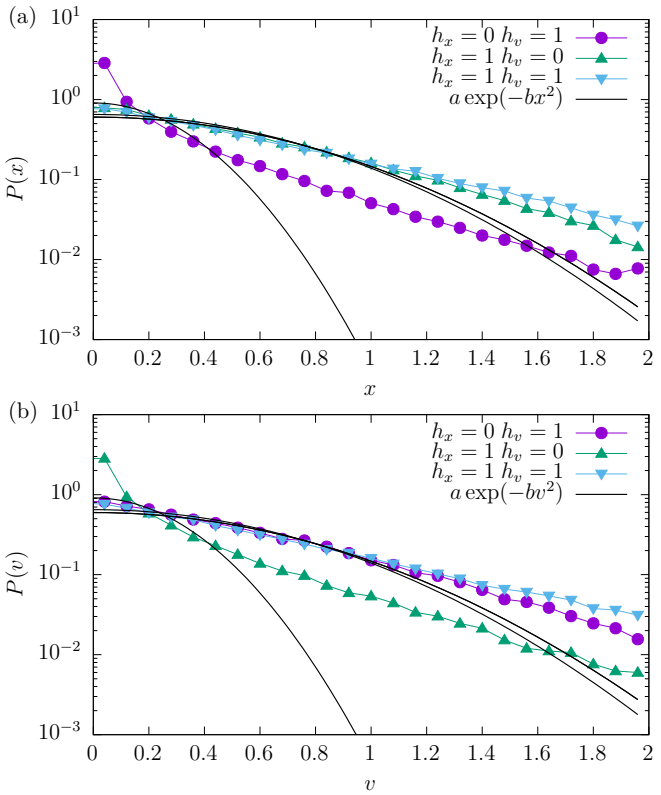

FIG. 9. Marginal nonequilibrium stationary densities corresponding to Fig. 8, i.e., $P(x)$ [top panel, (a)] and $P(v)$ [bottom panel, (b)] for the parabolic ($n = 1$) potential. Different curves correspond to different values of h_x and h_v. Solid lines represent $a_x \exp(-b_x x^2)$ and $a_v \exp(-b_v v^2)$ fits. Renewal intervals τ are distributed according to the half-normal distribution, see Eq. (31). Other parameters: $m = 1$ and $k = 1$.

i.e., for σ_r large enough, nonequilibrium stationary densities are not of BG type (results not shown). In particular, the distributions appear to have elongated tails compared with the BG distribution. In all the above-mentioned cases the nonequilibrium stationary states exist due to rapid decay of the tails of the renewal time distribution (faster than τ^{-2}); see [22] and [48].

Violations of the generalized equipartition relations visible in Figs. 6 and 7 are produced by resetting. The parameter σ_r controls the mean value and the variance of renewal intervals τ; see Eq. (31). It is responsible for the spreading of A_t and the increase in $\langle A_t \rangle$. To reintroduce equipartition relations, the parameter σ_r has to be large enough to increase the mean survival time (age) $\langle A_t \rangle$ beyond the transient oscillatory phase.

If we increase σ_r and consequently $\langle A_t \rangle$, the ratios of the average energies become closer to the predictions of Eqs. (21) and (22); see Figs. 10 and 11. Figures 10 and 11 show ratios of average energies for parabolic and quartic potentials as a function of the average age $\langle A_t \rangle$. These figures suggest that violation of generalized equipartition relations is caused by too frequent resets. Moreover, they indicate that if the average age $\langle A_t \rangle$ is longer than the duration of the transient phase, the generalized equipartition relations are recovered. For large enough $\langle A_t \rangle$, the generalized relations, see Eqs. (21) and (22), are in tact for all studied setups, i.e., also under the action of two noise sources; see Fig. 11. Therefore, for random resets the situation resembles the already discussed problem of ratios of energies at fixed times for equidistant resets; see Fig. 5. In Fig. 5, generalized equipartition holds (at reset time points) for large enough Δ.

If the variance, $\mathrm{var}(\tau) = \langle \tau^2 \rangle - \langle \tau \rangle^2$, of the renewal interval diverges, the average energy $\langle \mathcal{E}(t) \rangle$ no longer saturates but it starts to grow, because there is no stationary state in the system [48]. The energy growth cannot be faster than in the dynamics without resetting, which limits the overall growth rate. In particular, for $n = 1$ or any n with $h_x = 0$ the growth is sublinear, as the linear growth is the limiting growth that is recovered in the absence of resetting; see Eq. (16). To calculate the time dependence of the average energy, one needs to know the distribution $g(A_t)$ of the time since the last reset, i.e., the age at time t. The age A_t is given by $A_t = t - t_R$, where t_R is the last resetting (renewal) time. The age distribution fulfills [47]

$$P(A_t \leqslant s) = \begin{cases} F(t) - \int_0^{t-s} [1 - F(t-y)] dR(y), & s < t, \\ 1, & s \geqslant t, \end{cases} \tag{33}$$

where $F(t)$ is the renewal interval distribution $[F(t) = \int^t f(s)ds]$ and $R(t) = \langle N_t \rangle$ with $N_t := \max\{n \in \mathbb{N} : \sum_{i=1}^n \tau_i \leqslant t\}$. Now, the average energy can be calculated as

$$\langle \mathcal{E} \rangle = \Lambda \int_0^t g_t(s) s ds, \tag{34}$$

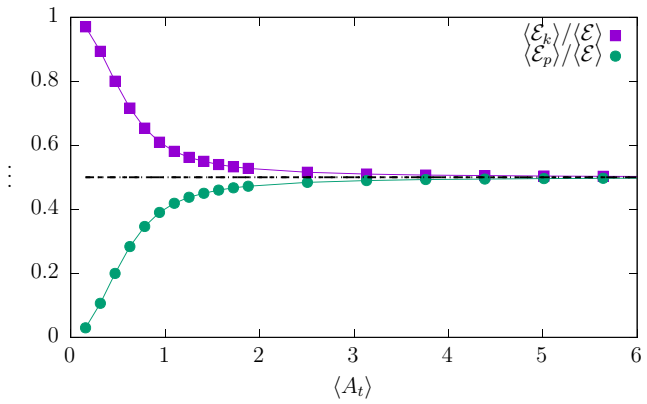

FIG. 10. Ratio of average energies for the parabolic ($n = 1$) potential with $(h_x, h_v) = (0, 1)$. Different curves correspond to $\langle\mathcal{E}_p\rangle/\langle\mathcal{E}\rangle$ and $\langle\mathcal{E}_k\rangle/\langle\mathcal{E}\rangle$. Dashed and dot-dashed lines depict theoretical ratios predicted by Eqs. (21) and (22). Renewal intervals τ are distributed according to the half-normal distribution, see Eq. (31). Other parameters: $m = 1$ and $k = 1$.

where

$$g_t(s) = \frac{dP}{ds} = \begin{cases} [1 - F(s)]R'(t-s), & s < t, \\ [1 - F(s)]R'(0)\delta(t-s), & s = t, \\ 0, & s > t. \end{cases} \tag{35}$$

If $\langle\tau\rangle$ is finite for $t \to \infty$, due to Blackwell's theorem [47], we can approximate $R(t)$ by $t/\langle\tau\rangle$ and $R'(t)$ by $\frac{1}{\langle\tau\rangle}$. Moreover, for the Pareto density [see Eq. (38)], characterized by the finite mean, we can calculate $R'(0)$, which is equal to 0, because

$$\frac{dR}{dt}(t) = \lim_{dt\to 0} \frac{\langle N_{t+dt}\rangle - \langle N_t\rangle}{dt}, \tag{36}$$

and for $dt < \delta$ we get $N_{0+dt} = 0$. Consequently, we have

$$\langle\mathcal{E}\rangle = \Lambda \int_0^t g_t(s) s\, ds = \frac{\Lambda}{\langle\tau\rangle} \int_0^t [1 - F(s)] s\, ds. \tag{37}$$

The estimate of $\langle\mathcal{E}(t)\rangle$ can be provided after selecting $f(\tau)$. Starting from now, for tractability reasons, we assume that renewal intervals follow Pareto's distribution ($\alpha > 0$, $\delta > 0$),

$$f(\tau) = \begin{cases} \frac{\alpha\delta^\alpha}{\tau^{\alpha+1}}, & \tau \geqslant \delta, \\ 0, & \tau < \delta, \end{cases} \tag{38}$$

with the cumulative density $F(\tau) = 1 - \delta^\alpha \tau^{-\alpha}$. The Pareto density is an example of the heavy-tailed, power-law distribution [48]. The average energy

$$\langle\mathcal{E}(t)\rangle = \Lambda \int_\delta^t g_t(s) s\, ds = \frac{\Lambda}{\langle\tau\rangle} \int_\delta^t [1 - F(s)] s\, ds \propto t^{2-\alpha}. \tag{39}$$

Consequently, for the Pareto renewal interval distribution with $1 < \alpha < 2$ the average energy grows as a power law with the exponent $2 - \alpha$. For $\alpha < 1$, the average renewal interval diverges and $R(t)$ cannot be approximated by $t/\langle\tau\rangle$. Nevertheless, we anticipate the linear growth of $\langle\mathcal{E}(t)\rangle$ as it is the limiting growth in the absence of resetting. The linear growth is already recovered for $\alpha \to 1^+$, as for $\alpha \to 1^+$ the exponent $2 - \alpha$ tends to 1; see Eq. (39).

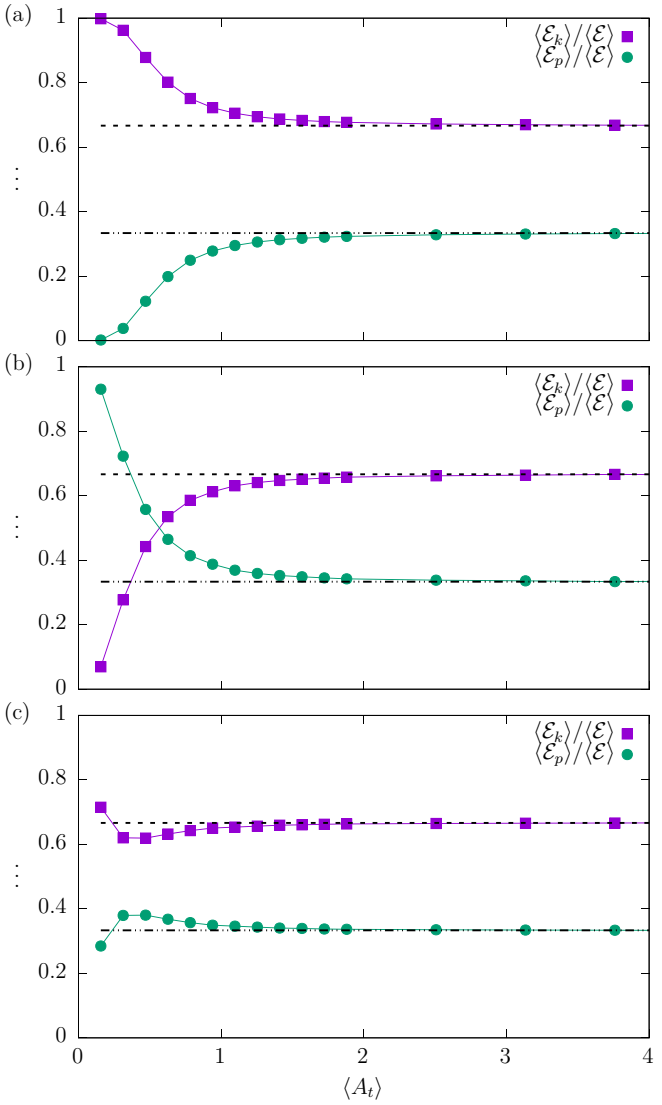

FIG. 11. The same as in Fig. 10 for the quartic ($n = 2$) potential with $(h_x, h_v) = (0, 1)$ [top panel, (a)], $(h_x, h_v) = (1, 0)$ [middle panel, (b)], and $(h_x, h_v) = (1, 1)$ [bottom panel, (c)]. Renewal intervals τ are distributed according to the half-normal distribution; see Eq. (31).

For comparison with numerical simulations, the top panel of Fig. 12 presents the time dependence of the average energy $\langle\mathcal{E}(t)\rangle$ for the parabolic potential with the Pareto distribution of renewal intervals with $1 < \alpha < 2$. Various curves correspond to various exponents α. For $1 < \alpha < 2$, the Pareto distribution is characterized by the finite mean renewal interval, but the variance of the renewal intervals diverges. Therefore, we are in the regime of validity of Eq. (39). The minimal renewal interval is set to $\delta = 0.01$. Additional parameters are equal to $m = 1$, $k = 4$. We show only results for $(h_x, h_v) = (0, 1)$, as for $(h_x, h_v) = (1, 0)$ and $(h_x, h_v) = (1, 1)$ the same scaling is recorded. Asymptotically, the average energy $\langle\mathcal{E}(t)\rangle$ scales in accordance to the predictions of Eq. (39), which are depicted by solid lines. Moreover, with decreasing α the quality of the $t^{2-\alpha}$ approximation improves. For α tending to 1^+ the $t^{2-\alpha}$ scaling approaches the linear scaling. The very

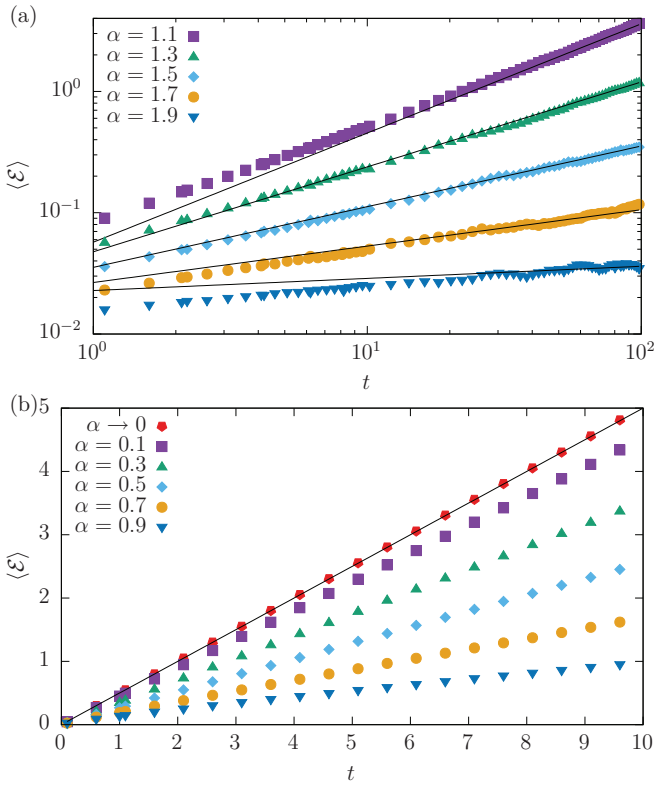

FIG. 12. Time dependence of average energies for the parabolic potential with $(h_x, h_v) = (0, 1)$ and the Pareto distribution, see Eq. (38), of renewal intervals with $1 < \alpha < 2$ [top panel, (a)] and $0 < \alpha < 1$ [bottom panel, (b)]. Various curves correspond to various values of the exponent α. Other parameters: $\delta = 0.01$, $k = 4$, and $m = 1$. Solid lines present the theoretical $t^{2-\alpha}$ scaling.

same scaling is recorded for average kinetic and potential energies (results not shown). For the quartic potential, the situation is more complex because average energies do not need to grow linearly in time. Nevertheless, for the fully traceable case of $h_x = 0$, we observe the same scaling as for the parabolic potential, i.e., $t^{2-\alpha}$ (results not shown).

The case of $\alpha < 1$ needs to be considered separately as for $\alpha < 1$ the mean renewal interval does not exist. For $\alpha < 1$, the linear scaling of the average energy is perfectly visible in the bottom panel of Fig. 12. The solid line in the bottom panel of Fig. 12 presents the $\langle \mathcal{E}(t) \rangle = \Lambda t$ line. In the limit of $\alpha \to 0$ there is no resetting. For $\alpha = 0.1$, the motion can still be reset but the dependence of $\langle \mathcal{E}(t) \rangle$ is very close to that without resetting. A change in α, as long as $\alpha < 1$, does not change the linear scaling, but changes the prefactor in the scaling.

For $\alpha < 1$, the ratios of average energies corresponding to the bottom panel of Fig. 12 asymptotically follow Eqs. (21) and (22) for all studied values of h_x and h_v (results not shown). The situation for $\alpha > 1$ is more complex. As all types of average energies display the same scaling, we expect a kind of generalized equipartition relations with the exact shape determined by the distribution of the renewal intervals. For $f(\tau)$ used in the top panel of Fig. 12, relations given by Eqs. (21) and (22) are recovered for $\alpha \to 1$. Otherwise, ratios of average energies are different. Violations of generalized equipartition relations are due to too frequent resets. Despite the fact that the Pareto density with $1 < \alpha < 2$ is characterized by the diverging variance, it still allows for frequent resetting. The number of very short renewal intervals can be reduced either by decreasing α or by increasing δ. Therefore, we have performed additional simulations with $\delta = 5$, which is well above the transient period. For $\delta = 5$, we have recovered equipartition relations (21) and (22) (results not shown). Here, the situation is similar to the one observed for $f(\tau) = \delta(\tau - \Delta)$ and $f(\tau)$ given by Eq. (31): too frequent resets introduce violations to equipartition relations.

III. SUMMARY AND CONCLUSIONS

Frictionless, noise driven dynamics in a single-well potential allow for unlimited growth of average energies. Here, we presented a possible mechanism that can assure the existence of nonequilibrium stationary states. The reintroduction of stationary states and bounding of energy is achieved by resetting the velocity and position at random time instants. If the variance of the renewal intervals is finite, the average energies are again finite and stationary states are reestablished. Contrary to the linear damping case, these states are not of the Boltzmann-Gibbs type. If the variance of the renewal intervals diverges, the systems still exhibit unbounded energy growth, yet it is slower than the limiting growth corresponding to the absence of resetting.

Using methods of statistical physics, it is possible to calculate the average kinetic and potential energies as a fraction of the average total energy. Here, we show that generalized equipartition relations hold also in setups for which a stationary state does not exist, e.g., in frictionless, noise-driven motions in single-well potentials. To observe generalized equipartition relations, the observation time needs to be longer than the transient period. Consequently, in frictionless dynamics, the average energies grow in an unlimited manner, but after the transient period their ratios become constant. The very same relations hold also when both velocity and position are perturbed by noise. Generalized equipartition relations are recovered in systems in which resets are not too frequent. This means, in practice, that for systems with resetting for which the nonequilibrium stationary state exists, the average time since the last reset has to be longer than the length of the transient period. If despite resetting there are no stationary states, which takes place if the variance of renewal interval diverges, generalized equipartition relations hold if short renewal intervals are excluded. This property is related to the fact that also in the absence of resetting, equipartition relations are observed after a transient period.

The studied model can be generalized in numerous ways. For example, it is possible to consider other types of resetting. For instance, one can reset the velocity or position only [49]. After such resetting, the system energy is reduced to kinetic or potential energies only. Therefore, initial conditions do not correspond to $\mathcal{E}_0 = 0$. On the one hand, such scenarios are capable of bounding energy growth. On the other hand, these resetting scenarios are not easily accessible analytically, as energy is not only determined by the time since the last reset, but also by the value of the energy after reset.

ACKNOWLEDGMENTS

This research project was supported in part by the PlGrid Infrastructure.

APPENDIX: EVOLUTION OF AVERAGE ENERGIES

From Eq. (13), i.e.,

$$\frac{dx(t)}{dt} = v(t) + \sqrt{h_x}\xi_x(t),$$
$$\frac{dv(t)}{dt} = -\gamma v(t) - \omega^2 x^{2n-1}(t) + \sqrt{h_v}\xi_v(t), \quad \text{(A1)}$$

it is possible to derive equations describing the time evolution of average kinetic $\langle \mathcal{E}_k \rangle$ and potential $\langle \mathcal{E}_p \rangle$ energies. Starting from $\mathcal{E}_p = k\frac{x^{2n}}{2n}$, we have

$$d\mathcal{E}_p = \frac{d\mathcal{E}_p}{dx}dx + \frac{1}{2}\frac{d^2\mathcal{E}_p}{dx^2}(dx)^2 + \cdots \quad \text{(A2)}$$
$$= kx^{2n-1}dx + \frac{1}{2}k(2n-1)x^{2n-2}(dx)^2$$

with

$$dx = vdt + \sqrt{h_x}dW_x, \quad \text{(A3)}$$

where dW_x stands for increments of the Wiener W_x process (Brownian motion). Analogously for $\mathcal{E}_k = \frac{1}{2}mv^2$, we have

$$d\mathcal{E}_k = \frac{d\mathcal{E}_k}{dv}dv + \frac{1}{2}\frac{d^2\mathcal{E}_k}{dv^2}(dv)^2 + \cdots \quad \text{(A4)}$$
$$= mvdv + \frac{1}{2}m(dv)^2$$

with

$$dv = -\gamma v dt - \omega^2 x^{2n-1}dt + \sqrt{h_v}dW_v, \quad \text{(A5)}$$

where dW_v represents increments of the Wiener process W_v. We assume that both processes W_x and W_v are independent, i.e., $\langle \xi_x(t)\xi_v(s)\rangle = 0$. Keeping terms that are at most linear in dt, we have

$$d\mathcal{E}_p = kx^{2n-1}vdt + \sqrt{h_x}kx^{2n-1}dW_x + \frac{1}{2}h_x k(2n-1)x^{2n-2}dt \quad \text{(A6)}$$

and

$$d\mathcal{E}_k = -m\gamma v^2 dt - m\omega^2 x^{2n-1}vdt + m\sqrt{h_v}vdW_v + \frac{1}{2}mh_v dt. \quad \text{(A7)}$$

From the above equations, we obtain the following formulas for time derivatives of average energies:

$$\frac{d}{dt}\langle \mathcal{E}_p(t)\rangle = k\langle x^{2n-1}v\rangle + \frac{1}{2}h_x k(2n-1)\langle x^{2n-2}\rangle \quad \text{(A8)}$$

and

$$\frac{d}{dt}\langle \mathcal{E}_k(t)\rangle = -m\gamma\langle v^2\rangle - m\omega^2\langle x^{2n-1}v\rangle + \frac{1}{2}mh_v, \quad \text{(A9)}$$

since the correlators $\langle x^{2n-1}dW_x\rangle$ and $\langle vdW_v\rangle$ vanish [45]. The change of total energy is described by

$$\frac{d}{dt}\langle \mathcal{E}(t)\rangle = \frac{d}{dt}\langle \mathcal{E}_p(t) + \mathcal{E}_k(t)\rangle \quad \text{(A10)}$$
$$= -m\gamma\langle v^2\rangle + \frac{1}{2}h_x k(2n-1)\langle x^{2n-2}\rangle + \frac{1}{2}mh_v.$$

Alternatively to the Itô lemma, one can use the method described in Chap. 3 of Ref. [45], which gives the same results.

[1] K. Sekimoto, *Stochastic Energetics* (Springer-Verlag, Berlin, 2010), Vol. 799.
[2] C. W. Gardiner, *Handbook of Stochastic Methods for Physics, Chemistry and Natural Sciences* (Springer-Verlag, Berlin, 2009).
[3] U. Seifert, Rep. Prog. Phys. **75**, 126001 (2012).
[4] W. Horsthemke and R. Lefever, *Noise-inducted Transitions. Theory and Applications in Physics, Chemistry, and Biology* (Springer-Verlag, Berlin, 1984).
[5] H. Risken, *The Fokker-Planck Equation: Methods of Solution and Applications* (Springer-Verlag, Berlin, 1996).
[6] L. E. Reichl, *A Modern Course in Statistical Physics* (Wiley, New York, 1998).
[7] F. Reif, *Fundamentals of Statistical and Thermal Physics* (Waveland, Long Grove, IL, 2009).
[8] K. Mallick and P. Marcq, Phys. Rev. E **66**, 041113 (2002).
[9] P. Hänggi, P. Talkner, and M. Borkovec, Rev. Mod. Phys. **62**, 251 (1990).
[10] L. Gammaitoni, P. Hänggi, P. Jung, and F. Marchesoni, Eur. Phys. J. B **69**, 1 (2009).
[11] T. Tomé and M. J. De Oliveira, *Stochastic Dynamics and Irreversibility* (Springer-Verlag, Berlin, 2016).
[12] R. Czopnik and P. Garbaczewski, Physica A **317**, 449 (2003).
[13] K. Mallick and P. Marcq, Eur. Phys. J. B **31**, 553 (2003).
[14] K. Mallick and P. Marcq, J. Phys. A **37**, 4769 (2004).
[15] M. Majka and P. F. Góra, Phys. Rev. E **94**, 042110 (2016).
[16] A. Janicki and A. Weron, *Simulation and Chaotic Behavior of α-stable Stochastic Processes* (Marcel Dekker, New York, 1994).
[17] A. A. Dubkov, B. Spagnolo, and V. V. Uchaikin, Int. J. Bifurcation Chaos. Appl. Sci. Eng. **18**, 2649 (2008).
[18] A. V. Chechkin, J. Klafter, V. Y. Gonchar, R. Metzler, and L. V. Tanatarov, Phys. Rev. E **67**, 010102(R) (2003).
[19] B. Dybiec, E. Gudowska-Nowak, and I. M. Sokolov, Phys. Rev. E **76**, 041122 (2007).
[20] I. M. Sokolov, W. Ebeling, and B. Dybiec, Phys. Rev. E **83**, 041118 (2011).
[21] B. Dybiec, E. Gudowska-Nowak, and I. M. Sokolov, Phys. Rev. E **96**, 042118 (2017).
[22] M. R. Evans, S. N. Majumdar, and G. Schehr, J. Phys. A: Math. Theor. **53**, 193001 (2020).
[23] M. R. Evans and S. N. Majumdar, Phys. Rev. Lett. **106**, 160601 (2011).
[24] Ł. Kuśmierz and E. Gudowska-Nowak, Phys. Rev. E **92**, 052127 (2015).

[25] S. Eule and J. J. Metzger, N. J. Phys. **18**, 033006 (2016).
[26] E. Gelenbe, Phys. Rev. E **82**, 061112 (2010).
[27] S. Gupta, S. N. Majumdar, and G. Schehr, Phys. Rev. Lett. **112**, 220601 (2014).
[28] J. M. Meylahn, S. Sabhapandit, and H. Touchette, Phys. Rev. E **92**, 062148 (2015).
[29] S. C. Manrubia and D. H. Zanette, Phys. Rev. E **59**, 4945 (1999).
[30] M. R. Evans and S. N. Majumdar, J. Phys. A **44**, 435001 (2011).
[31] A. Pal, Phys. Rev. E **91**, 012113 (2015).
[32] E. Sparre Andersen, Math. Scand. **1**, 263 (1953).
[33] E. Sparre Andersen, Math. Scand. **2**, 194 (1954).
[34] A. V. Chechkin *et al.*, J. Phys. A **36**, L537 (2003).
[35] M. Mandrysz and B. Dybiec, Acta Phys. Pol. B **49**, 871 (2018).
[36] M. Mandrysz and B. Dybiec, Phys. Rev. E **99**, 012125 (2019).
[37] M. Gitterman, *The Noisy Oscillator: The First Hundred Years, from Einstein until Now* (World Scientific, Singapore, 2005).
[38] M. Gitterman, *The Noisy Oscillator: Random Mass, Frequency, Damping* (World Scientific, Singapore, 2013).
[39] R. Kubo, Rep. Prog. Phys. **29**, 255 (1966).
[40] H. Risken, *The Fokker-Planck Equation. Methods of Solution and Application* (Springer-Verlag, Berlin, 1984).
[41] M. Mandrysz and B. Dybiec, J. Phys. A: Math. Theor. **53**, 195001 (2020).
[42] H. Goldstein, C. Poole, and J. Safko, *Classical Mechanics* (Pearson, Essex, UK, 2002).
[43] A. Fuliński and P. F. Góra, J. Stat. Phys. **101**, 483 (2000).
[44] X. Mao, *Stochastic Differential Equations and Applications* (Woodhead, Oxford, 2007).
[45] T. Tomé and M. J. de Oliveira, *Stochastic Dynamics and Irreversibility* (Springer-Verlag, Berlin, 2015).
[46] S. Albeverio and A. Klar, J. Math. Phys. **35**, 4005 (1994).
[47] L. Breuer and D. Baum, *An Introduction to Queueing Theory and Matrix-analytic Methods* (Springer, Dordrecht, 2005).
[48] A. Nagar and S. Gupta, Phys. Rev. E **93**, 060102(R) (2016).
[49] D. Gupta, J. Stat. Mech. (2019) 033212.